Materials Science in Additive Manufacturing

ORIGINAL RESEARCH ARTICLE

Experimental and numerical studies on the acoustic performance of simple cubic structure lattices fabricated by digital light processing

Supplementary File

Supplementary Text 1

Section 1 – Review of the merits and demerits of the commercialized additive manufacturing technologies

Table S1. Categories and merits and demerits of the AM technologies

Category	Technology	Material form	Material category	Merits	Demerits
Liquid-based additive manufacturing	Stereolithography	Liquid	Photopolymer	• Automatic operation • Varying build volumes • Good accuracy • Best surface finish • Wild range of materials	• Require support structures • Require post-processing • Require post-curing
	PolyJet		Photopolymer; thermoplastics	• High printing quality • High dimension accuracy • Fast process speed • Smooth surface finish • Wide range of materials • Easy usage • Safe and clean process • Combination of the materials	• Require post-processing • Material wastage
	MultiJet		UV curable liquid plastics; thermos-polymers	• Efficient and ease of use • High precision of printing • Cost-effective modelling • Fast build time • Office friendly process	• Small build volume • Limited materials
	Digital light processing		Photopolymer	• High building speed • Office friendly process • Small quantity of resin during build • No wiper or leveler • Less shrinkage	• Limited building volumes • Peeling of the completed part • Require post-processing
	3D bioprinting		Bioink and tissues	• Unique technology for biofield • Cost-effective	• Small building volume • Sterile environment
	Rapid freeze prototyping		Water and eutectic sugar solution	• Low running cost • Good accuracy • Good building speed • Environmentally friendly materials	• Require cold environment • Need additional processing • Unrepeatability • Require post-processing
	Aerosol jet		Suspended and atomized source materials	• Planar and non-planar (3D) printing capabilities • Large printed feature sizes • Thin layer deposition • A wide range of inks and substrates • Low-temperature processing	• Small particle size limitation • Low resolution for current nozzle spacing
	Two-photon Polymerization		Photosensitive/ photoresist	• Direct fabrication of arbitrary 3D microstructures	• Lack of scalability • Negative effects accompanied

(Contd...)

Table S1. ***(Continued)***

Category	Technology	Material form	Material category	Merits	Demerits
			materials	• Infrared light induced polymerization • Good structure resolution and quality	by high resolution
	Ceramics additive manufacturing		Photosensitive resin and ceramic particles	• High resolution and precision • No minimum quantity thresholds • Flexibility and high speed • Same properties as parts made in a traditional way • High efficiency	• Long post-processing time • Large shrinkage • No multi-color or multi-material capabilities
Solid-based additive manufacturing	Fused deposition modelling	Solid	Thermoplastics	• Fabrication of functional parts • Minimal wastage • Ease of support removal • Ease of material change • Large build volume	• Restricted accuracy • Slow process • Unpredictable shrinkage
	Selective deposition lamination		Paper	• Low cost • High precision • Safety • Ecofriendly • High resolution in color printing	• Low strength • Small build volume
	Electron beam additive manufacturing		Weldable metals	• Non-flammability • Low material wastage • Low cost • Varying material composition • Switching between fine and coarse features • High deposition rates	• Inability to print overhangs • Poor resolution • Limited materials
	Selective laser sintering	Powder	Thermoplastics	• Good part stability • Wide range of processing materials • No part supports required • Little post-processing required • No post-curing required	• Large physical size of the unit • High power consumption • Poor surface finish
	Selective laser melting		Metal	• High-quality metal parts • Large range of metal materials • Relatively lesser processes and low cost • High accuracy • Complex geometries	• Large physical size of the unit • High power consumption • Relatively slow process
	ColorJet printing		VisiJet PXL	• High speed • Versatile • Simple to operate • Minimal wastage of materials • Customized color	• Limited functional parts • Poor surface finish
	Laser metal deposition		Metallic materials	• Superior material properties • Add material onto existing parts • Enable blend materials • Low powder cost • Large working area	• Geometrical complexity • Surface finish • Dimensional accuracy
	Electron beam melting		Metallic materials	• Superior material properties • Excellent accuracy • Excellent finishing • Good build speed	• Need to maintain the vacuum chamber • High power consumption • Gamma ray generation
	Hybrid AM		Metallic materials	• Hybrid CAD/CAM in one run • Relatively fast process • Build 3D-contours without support structure	• Lack of fully developed materials • Limitation of material choices

(Contd...)

Table S1. ***(Continued)***

Category	Technology	Material form	Material category	Merits	Demerits
				• Flexible changeover between additive and subtractive processes • Possibility of thin-walled structure • Closed-loop control • Multi-materials are possible	
	Digital part materialization		Metallic materials	• Fast • Flexible • Reliable • Large parts	• Large space required • Limited materials
	Multi jet fusion		N. A.	• Fast • Low cost per part • High-quality functional parts • High accuracy and fine details • Add additional parts in the midst of printing	• Restriction by STL format • Need of post-processing • Limited variations of materials

Supplementary Text 2

Section 2.3 – Information on the calculated parameters of the Delany-Bazley (DB) model and the multi-layered micropore-cavity (MMC) model

Table S2. Design and mathematical model parameters of samples

Sample	Strut length D (mm)	Strut width R (mm)	Air volume V_a (mm^3)	Wetted surface area A_{sf} (mm^2)	Porosity φ	Tortuosity χ	Representative unit cell (RUC) dimension d_{RUC} (mm)	Airflow resistivity σ (Pa.s.m–^{2})	Tube side length d_{tube}	Tube thickness d_{tube} (mm)	Cavity layer thickness l_{cau} (mm)	Perforation ratio ε
1	3.0	0.43	22.67	44.56	0.8396	1.5073	1.6421	267.89	2.14	0.30	2.39	0.5088
2	3.0	0.63	18.61	57.99	0.6893	1.7419	1.7644	582.00	1.74	0.45	2.11	0.3364
3	3.0	0.83	13.99	66.78	0.5181	1.9758	1.9717	1230.26	1.34	0.59	1.83	0.1995
4	5.0	0.63	109.13	111.98	0.8730	1.4459	2.6979	77.40	3.74	0.45	4.11	0.5595
5	5.0	0.83	99.01	137.91	0.7921	1.5871	2.7961	126.51	3.34	0.59	3.83	0.4462
6	5.0	1.03	87.37	159.21	0.6990	1.7280	2.9248	200.48	2.94	0.73	3.54	0.3457
7	5.0	1.23	74.76	175.87	0.5981	1.8685	3.1009	314.21	2.54	0.87	3.26	0.2581
8	5.0	1.43	61.72	187.89	0.4938	2.0083	3.3553	491.36	2.14	1.01	2.98	0.1832
9	6.0	0.83	183.51	173.48	0.8496	1.4896	3.2703	62.91	4.34	0.59	4.83	0.5232
10	6.0	1.03	168.37	203.34	0.7795	1.6071	3.3744	93.93	3.94	0.73	4.54	0.4312
11	6.0	1.23	151.50	228.57	0.7014	1.7245	3.5052	137.67	3.54	0.87	4.26	0.3481
12	6.0	1.43	133.45	249.17	0.6178	1.8416	3.6749	200.24	3.14	1.01	3.98	0.2739
13	6.0	1.63	114.75	265.12	0.5313	1.9583	3.9025	290.79	2.74	1.15	3.69	0.2085
14	6.0	1.83	95.96	276.45	0.4443	2.0745	4.2240	421.55	2.34	1.29	3.41	0.1521
15	7.5	1.03	359.25	269.54	0.8515	1.4860	4.0845	39.76	5.44	0.73	6.04	0.5261
16	7.5	1.23	335.99	307.63	0.7964	1.5801	4.1854	54.94	5.04	0.87	5.76	0.4516
17	7.5	1.43	310.42	341.08	0.7358	1.6741	4.3063	74.85	4.64	1.01	5.48	0.3827
18	7.5	1.63	283.07	369.89	0.6710	1.7679	4.4532	101.27	4.24	1.15	5.19	0.3196
19	7.5	1.83	254.50	394.07	0.6032	1.8615	4.6359	136.55	3.84	1.29	4.91	0.2621
20	7.5	2.03	225.23	413.61	0.5339	1.9548	4.8682	184.04	3.44	1.44	4.63	0.2104
21	7.5	2.23	195.83	428.52	0.4642	2.0478	5.1737	247.78	3.04	1.58	4.35	0.1643

https://doi.org/10.18063/msam.v1i4.22

Supplementary Text 3

Section 3.1 – Macroscopic sample images for SC-lattice samples

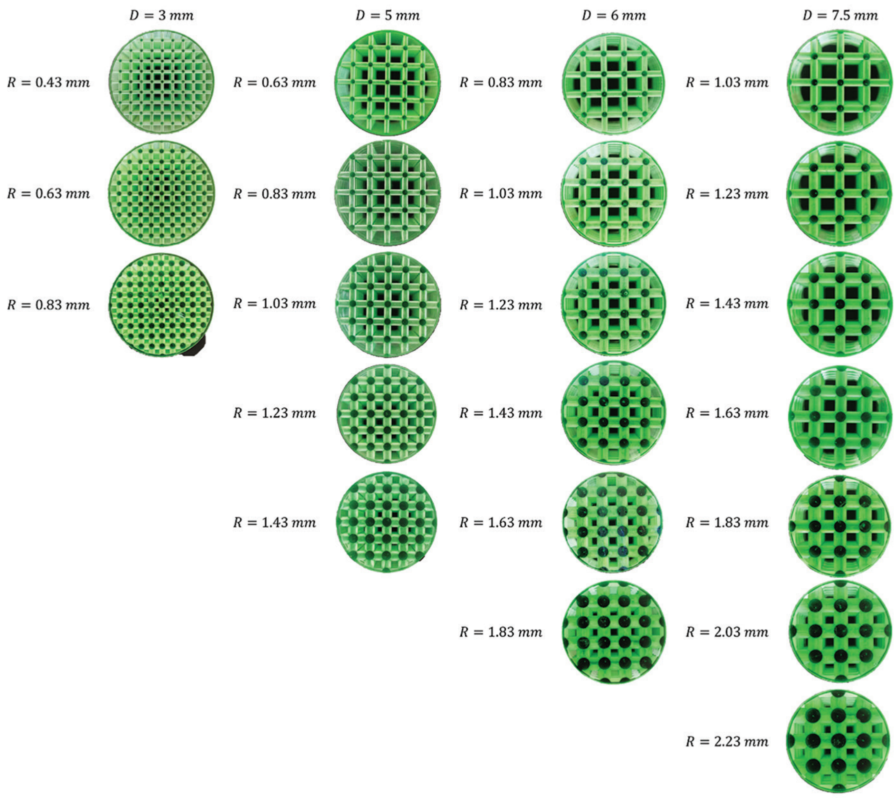

Figure S1. Macroscopic sample images for SC-Truss lattices samples in this work.

Supplementary Text 4

Section 3.1 – Microscopic sample images for SC-lattice samples

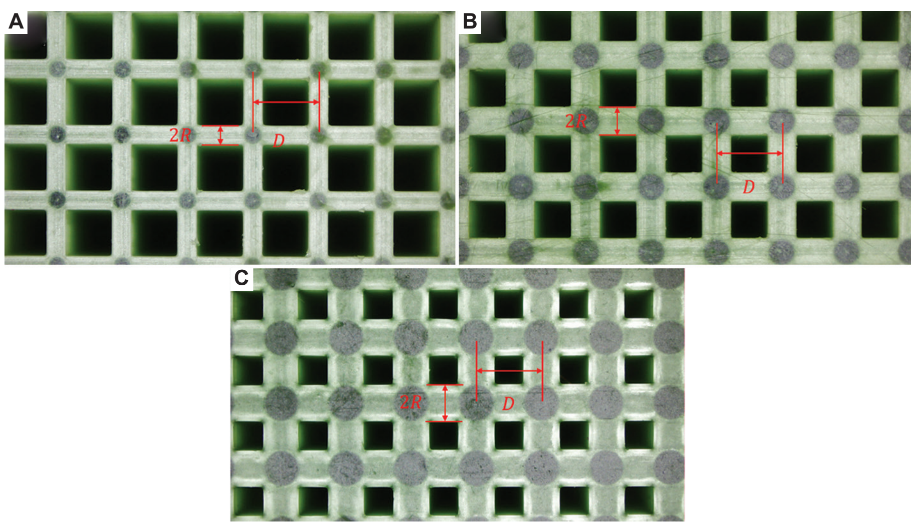

Figure S2. Microscopic sample images (strut length D and strut width R) for SC-Truss lattices with strut length of 3 mm and strut widths of (A) 0.43 mm, (B) 0.63 mm, and (C) 0.83 mm, respectively.

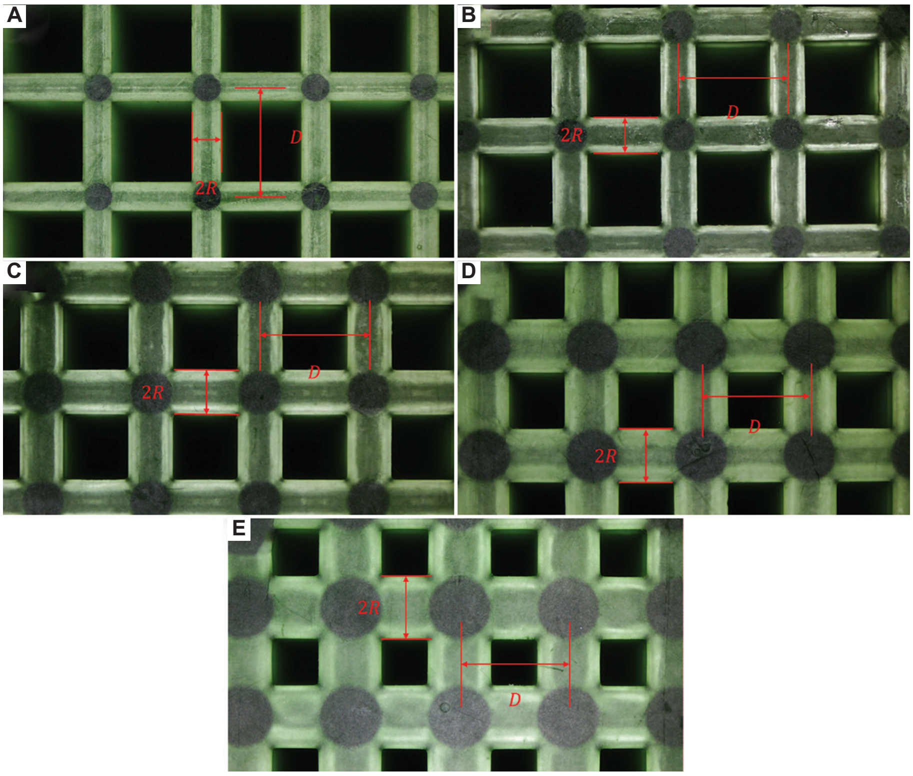

Figure S3. Microscopic sample images (strut length *D* and strut width *R*) for SC-Truss lattices with strut length of 5 mm and strut widths of (A) 0.63 mm, (B) 0.83 mm, (C) 1.03 mm, (D) 1.23 mm, and (E) 1.43 mm, respectively.

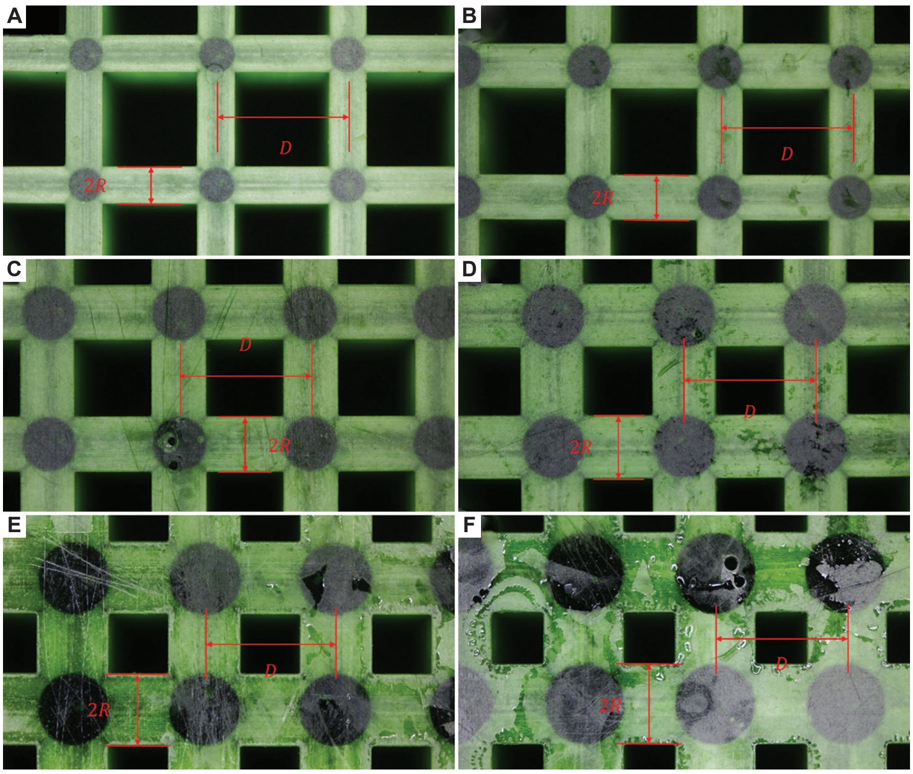

Figure S4. Microscopic sample images (strut length *D* and strut width *R*) for SC-Truss lattices with strut length of 6 mm and strut widths of (A) 0.83 mm, (B) 1.03 mm, (C) 1.23 mm, (D) 1.43 mm, (E) 1.63 mm, and (F) 1.83 mm, respectively.

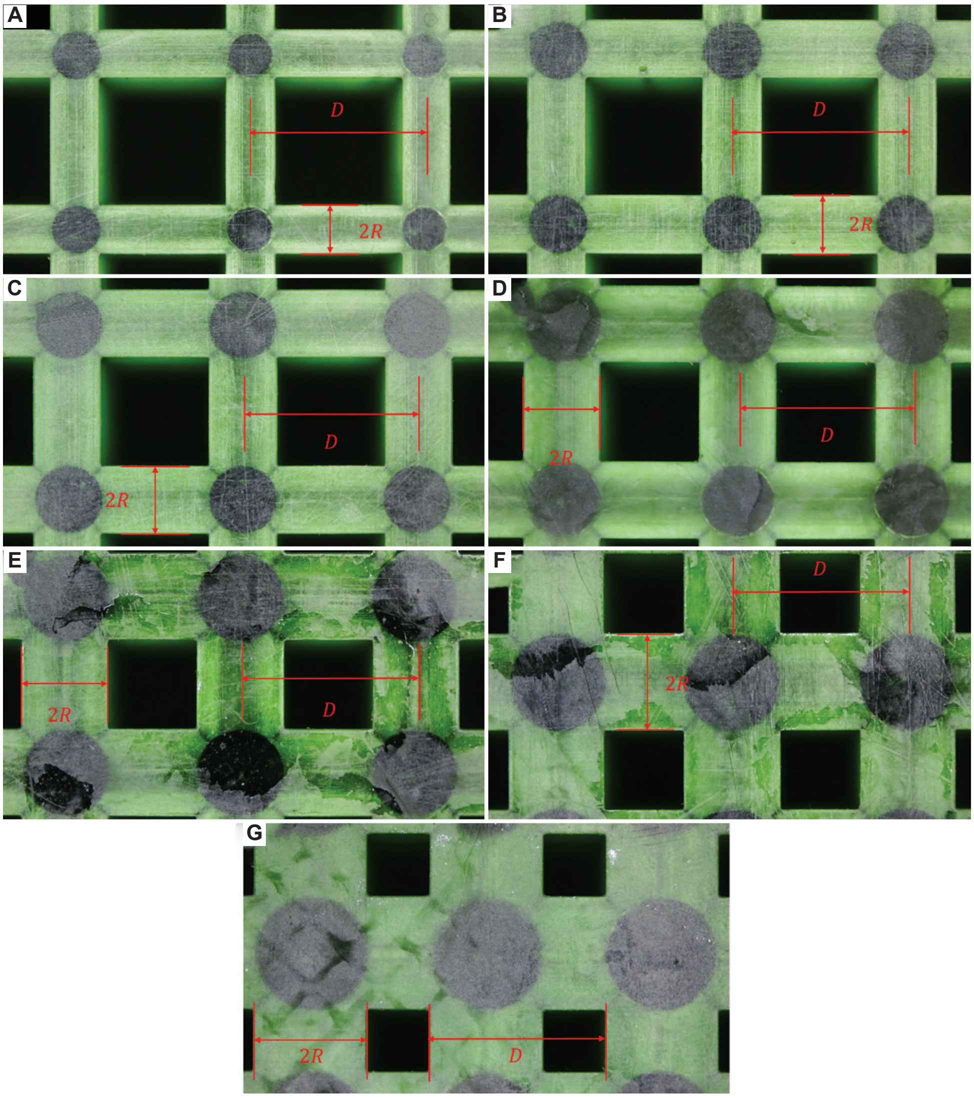

Figure S5. Microscopic sample images (strut length *D* and strut width *R*) for SC-Truss lattices with strut length of 7.5 mm and strut widths of (A) 1.03 mm, (B) 1.23 mm, (C) 1.43 mm, (D) 1.63 mm, (E) 1.83 mm, (F) 2.03 mm, and (G) 2.23 mm, respectively.

Supplementary Text 5

Section 3.3.1 – The comparison plots between experiments and Delany-Bazley model for all the test cases in this work

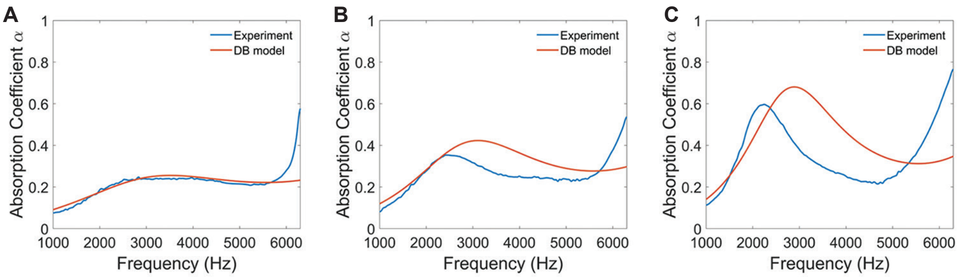

Figure S6. Plot of the sound absorption coefficients obtained both experimentally and calculated using the Delany-Bazley model for SC-Truss lattices with strut length of 3 mm and strut widths of (A) 0.43 mm, (B) 0.63 mm, and (C) 0.83 mm, respectively.

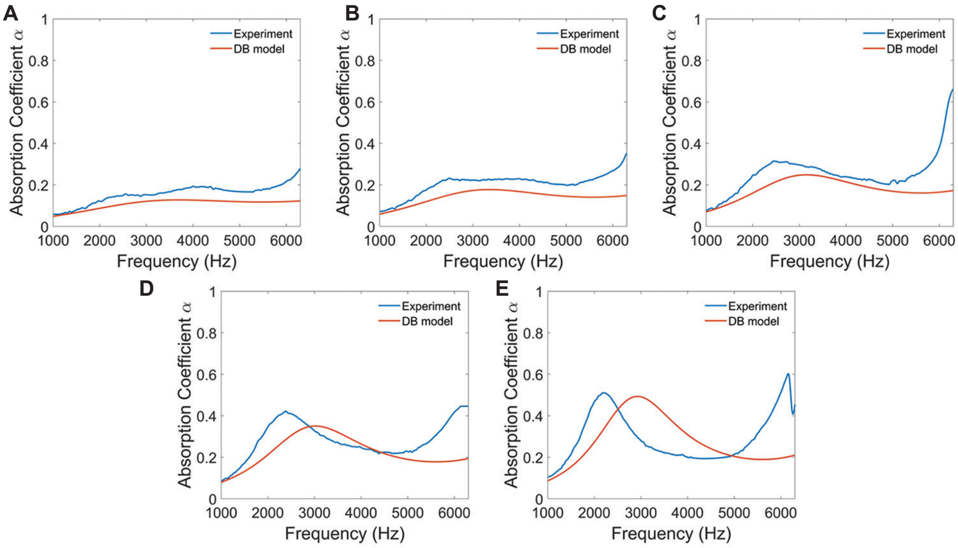

Figure S7. Plot of the sound absorption coefficients obtained both experimentally and calculated using the Delany-Bazley model for SC-Truss lattices with strut length of 5 mm and strut widths of (A) 0.63 mm, (B) 0.83 mm, (C) 1.03 mm, (D) 1.23 mm, and (E) 1.43 mm, respectively.

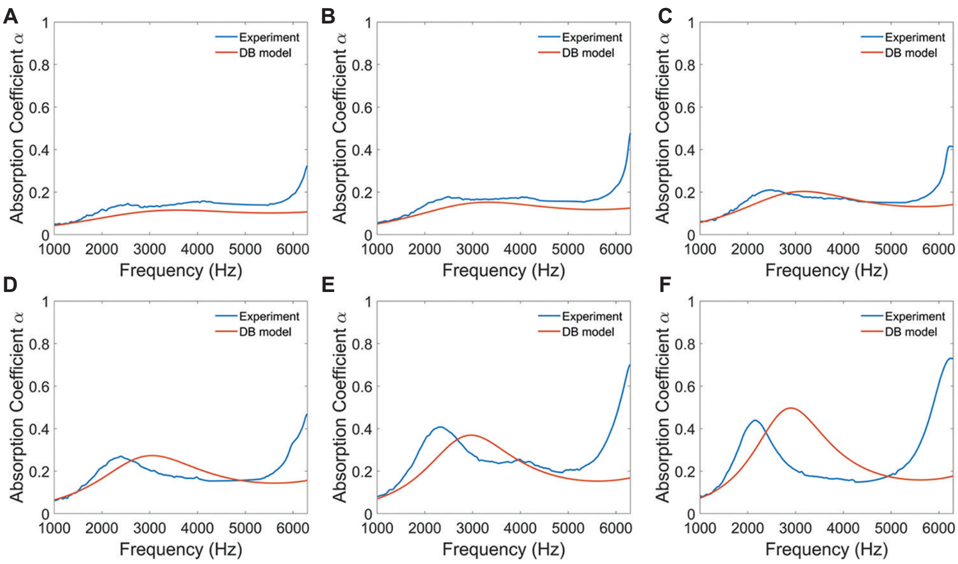

Figure S8. Plot of the sound absorption coefficients obtained both experimentally and calculated using the Delany-Bazley model for SC-Truss lattices with strut length of 6 mm and strut widths of (A) 0.83 mm, (B) 1.03 mm, (C) 1.23 mm, (D) 1.43 mm, (E) 1.63 mm, and (F) 1.83 mm, respectively.

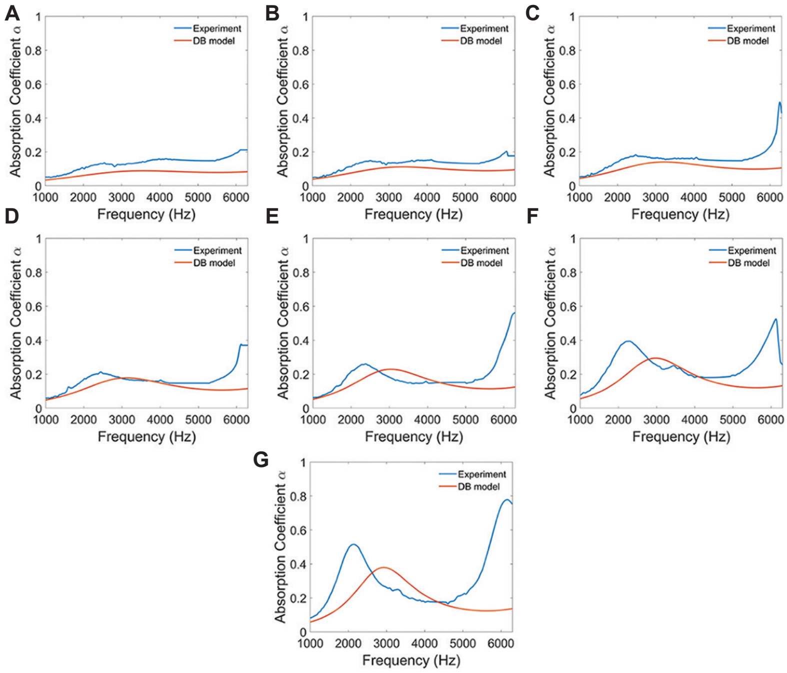

Figure S9. Plot of the sound absorption coefficients obtained both experimentally and calculated using the Delany-Bazley model for SC-Truss lattices with strut length of 7.5 mm and strut widths of (A) 1.03 mm, (B) 1.23 mm, (C) 1.43 mm, (D) 1.63 mm, (E) 1.83 mm, (F) 2.03 mm, and (G) 2.23 mm, respectively.

Supplementary Text 6

Section 3.3.3 – Values of the correction factors δ1 and δ2 for the multi-layered micropore-cavity model

Table S3. Values of the correction factors δ1 and δ2 for the MMC model

Sample	Strut length *D* (mm)	Strut width *R* (mm)	δ_1	δ_2
1	3.0	0.43	40	0.2
2	3.0	0.63	18	0.35
3	3.0	0.83	6	0.1
4	5.0	0.63	100	0.1
5	5.0	0.83	80	0.35
6	5.0	1.03	60	0.3
7	5.0	1.23	40	0.2
8	5.0	1.43	12	0.05
9	6.0	0.83	100	0.15
10	6.0	1.03	80	0.3
11	6.0	1.23	40	0.3
12	6.0	1.43	20	0.3
13	6.0	1.63	20	0.1
14	6.0	1.83	8	0
15	7.5	1.03	200	0.3
16	7.5	1.23	100	0.15
17	7.5	1.43	80	0.3
18	7.5	1.63	60	0.25
19	7.5	1.83	40	0.25
20	7.5	2.03	40	0.05
21	7.5	2.23	20	0

MMC: Multi-layered micropore-cavity

Supplementary Text 7

Section 3.3.2 – The comparison plots between experiments and multi-layered micropore-cavity model for all the test cases in this work

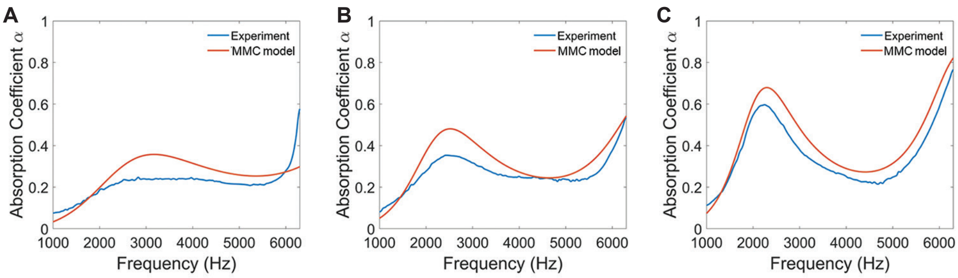

Figure S10. Plot of the sound absorption coefficients obtained both experimentally and calculated using the multi-layered micropore-cavity model for SC-Truss lattices with strut length of 3 mm and strut widths of (A) 0.43 mm, (B) 0.63 mm, and (C) 0.83 mm, respectively.

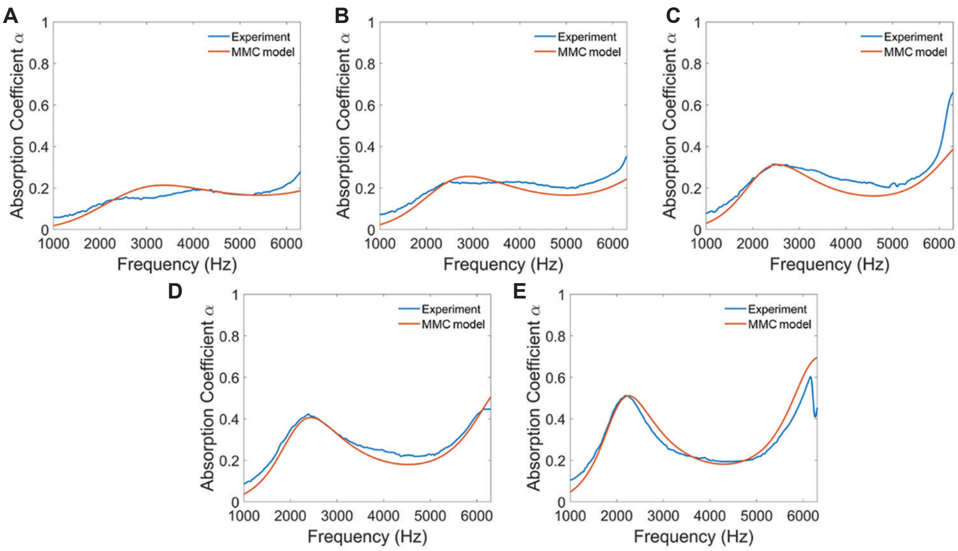

Figure S11. Plot of the sound absorption coefficients obtained both experimentally and calculated using the multi-layered micropore-cavity model for SC-Truss lattices with strut length of 5 mm and strut widths of (A) 0.63 mm, (B) 0.83 mm, (C) 1.03 mm, (D) 1.23 mm, and (E) 1.43 mm, respectively.

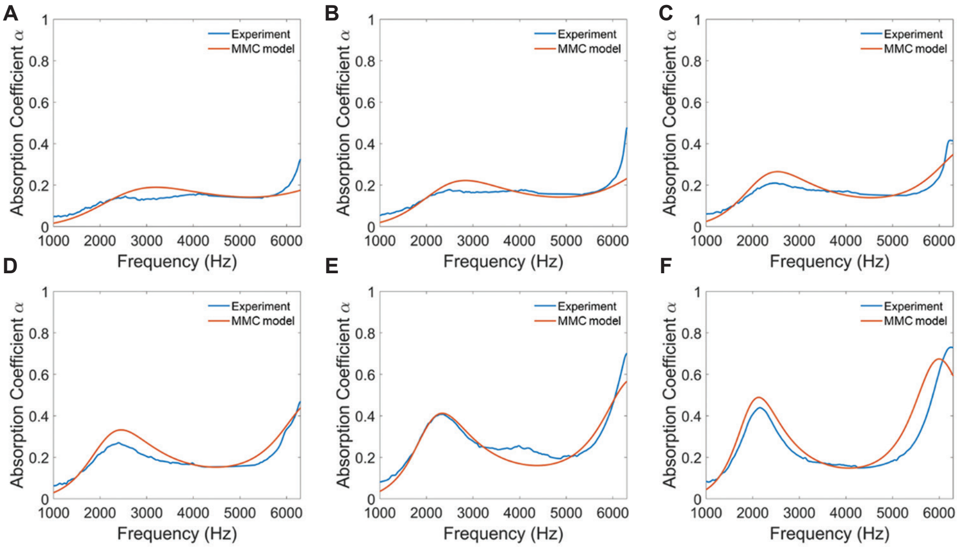

Figure S12. Plot of the sound absorption coefficients obtained both experimentally and calculated using the multi-layered micropore-cavity model for SC-Truss lattices with strut length of 6 mm and strut widths of (A) 0.83 mm, (B) 1.03 mm, (C) 1.23 mm, (D) 1.43 mm, (E) 1.63 mm, and (F) 1.83 mm, respectively.

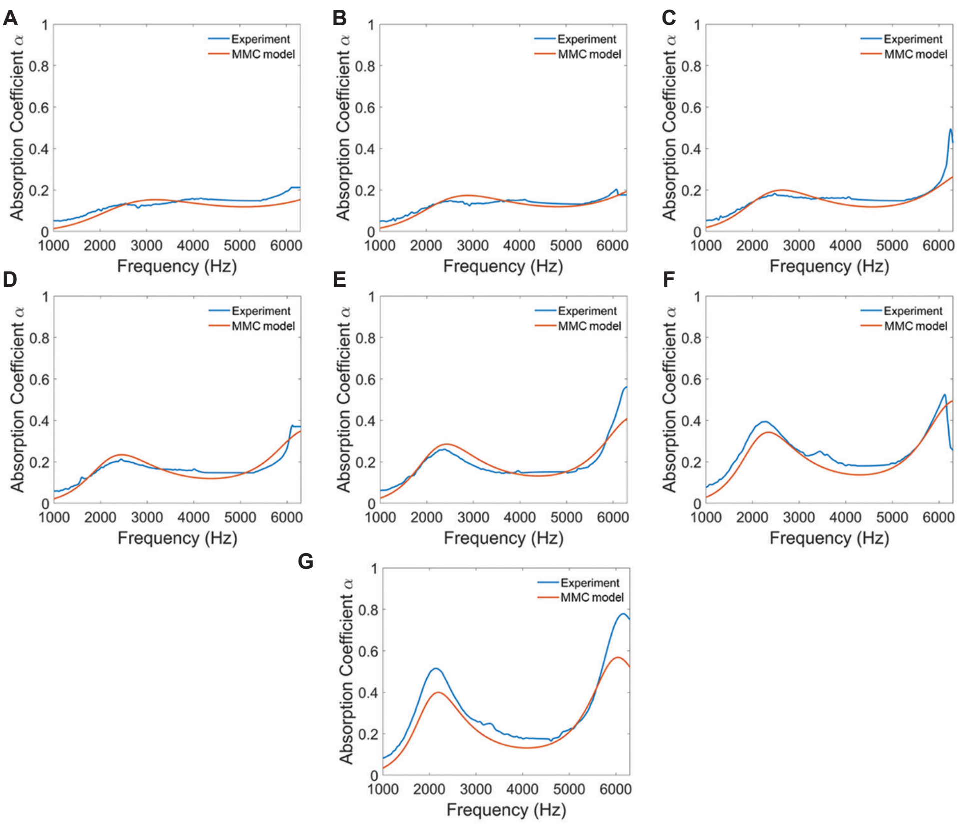

Figure S13. Plot of the sound absorption coefficients obtained both experimentally and calculated using the multi-layered micropore-cavity model for SC-Truss lattices with strut length of 7.5 mm and strut widths of (A) 1.03 mm, (B) 1.23 mm, (C) 1.43 mm, (D) 1.63 mm, (E) 1.83 mm, (F) 2.03 mm, and (G) 2.23 mm, respectively.

Supplementary Text 8

Section 3.3.3 – Values of the mean percentage errors of the absorption coefficients based on the Delany-Bazley model and the multi-layered micropore-cavity model

Table S4. Mean percentage errors in absorption coefficients based on the Delany-Bazley model and the multi-layered micropore-cavity model

Sample	Strut length *D* (mm)	Strut width *R* (mm)	Porosity φ	Mean percentage errors in absorption coefficients	
				Delany-Bazley model	Multi-layered micropore-cavity model
1	3.0	0.43	0.8396	8.58	26.72
2	3.0	0.63	0.6893	25.33	20.36
3	3.0	0.83	0.5181	45.24	19.00
4	5.0	0.63	0.8730	28.31	17.41
5	5.0	0.83	0.7921	28.84	18.30
6	5.0	1.03	0.6990	24.44	18.09
7	5.0	1.23	0.5981	22.84	12.59
8	5.0	1.43	0.4938	41.31	12.14
9	6.0	0.83	0.8496	25.66	17.95
10	6.0	1.03	0.7795	21.20	15.69
11	6.0	1.23	0.7014	14.03	16.31
12	6.0	1.43	0.6178	23.09	15.69
13	6.0	1.63	0.5313	27.35	13.33
14	6.0	1.83	0.4443	55.73	20.19
15	7.5	1.03	0.8515	42.00	21.96
16	7.5	1.23	0.7964	29.93	15.10
17	7.5	1.43	0.7358	28.87	15.59
18	7.5	1.63	0.6710	22.37	15.29
19	7.5	1.83	0.6032	28.02	14.20
20	7.5	2.03	0.5339	32.29	18.31
21	7.5	2.23	0.4642	42.19	20.35